Detection of energy-selected secondary electrons in coincidence with energy-loss events in thin carbon foils

Folbert J. Pijper and Pieter Kruit
Department of Applied Physics, Delft University of Technology, Lorentzweg 1, 2628 CJ Delft, The Netherlands
(Received 3 May 1991)

The ultimate resolution in secondary-electron images obtained in a scanning transmission electron microscope depends strongly on secondary-electron-production mechanisms. In such a microscope, equipped with an electron-energy-loss spectrometer as well as a secondary-electron-energy analyzer, coincidences have been achieved between secondary electrons and energy-loss electrons. This has resulted in additional information on the origin of secondary electrons in thin carbon films. The average probability for the production of secondary electrons of a given kinetic energy rises linearly with the energy lost by the primary electrons minus this kinetic energy and a few eV. These secondary electrons seem to appear from a cascade which was started by the original energy-loss event. Since most of these events are volume-plasmon excitations, volume-plasmon decay followed by a cascade contributes strongly to the secondary-electron emission. The linear relation seems to break down at energy losses of more than $\approx$ 125 eV. Energy losses associated with surface plasmons give a high probability for emission and detection of secondary electrons with a kinetic energy of 2–3 eV. For losses which are about 11 eV higher than the kinetic energy of the secondary electrons, an enhanced probability of emission exists. This enhancement is attributed to direct ionization from the valence band. The results are obtained in non-ultrahigh-vacuum conditions but show one of the many possibilities of coincidence spectroscopy in a scanning transmission electron microscope.

I. INTRODUCTION

The impact of a primary electron on a specimen in the electron microscope can cause several scattering events. If more than one scattering product is detected, additional information on the scattering event and thus on the specimen can be extracted. Coincidence techniques are required to find out which scattering products belong together. They rely on the fact that the creation of a secondary particle by an energy-loss process of the primary electron occurs almost immediately. We report on preliminary coincidence experiments between secondary electrons and the transmitted energy-loss electrons. The results are preliminary since only in a later stage ultrahigh-vacuum (UHV) conditions, high spatial resolution, and other energy ranges will be available. Nevertheless, these results give indications on the origin of secondary electrons. Before describing the experiment and the results we shall give a short review of related coincidence work.

Most early coincidence spectroscopy studies were performed on gases. Van der Wiel and Brion[1] have reported on so-called near-dipole $(e,2e)$ spectroscopy experiments, which rely on the similarity with photo electron spectroscopy or the theoretical correspondence between photon- and electron-induced excitations; see, e.g., Jackson.[2] The significance of $(e,2e)$ spectroscopy or any coincidence spectroscopy in which the electron-energy-loss spectroscopy (EELS) signal is involved, is best understood if we interpret the absorption of energy from the primary electron as a virtual photon: by the impact of the primary electron the secondary electron can obtain a kinetic energy, equal to the difference of the energy loss and its original binding energy.

Coincidence spectroscopy has been used by Ungier and Thomas[3] to decompose the Auger spectrum in specific Auger decay processes, by acquiring the Auger electrons in coincidence with certain well-defined energy losses.

If both energy and direction of the scattering products is available, the original momentum distribution of the ejected electrons can be found. Normally this is done with lower primary energies and consequently larger scattering angles. McCarthy and Weigold[4] have reviewed studies aimed at the reconstruction of this distribution. Most of these experiments are done on gases, some on solids.

The study of solids has always been more complicated. In a solid, before escaping from the surface, an unknown amount of energy can be lost in a "cascade" of subsequent scattering events. Besides this, the work function must be overcome. Some electrons of the original energy distribution will have moved toward the low-energy part of the spectrum; others will not escape.

Haak *et al.*[5] used Auger-photoelectron coincidence spectroscopy (APECS) to study solids. The energy of the (x-ray excited) photoelectron defines the intermediate state in the Auger process. The decay from these states shows up in the APECS spectrum.

Ritter, Dennison, and Jones[6] measured the spectral momentum density of the valence band of amorphous carbon by $(e,2e)$ spectroscopy, using 25-keV electrons and scattering angles close to 45°. Two separate bands (energy against momentum transfer) were distinguished. One band extends from 10 to 23 eV; the other is situated at about 9-eV binding energy. This indicates the possible occurrence of different bonding types between the carbon atoms in the film. More recent work by Gao *et al.*[7] and

Hayes and co-workers[8,9] on evaporated carbon, graphite, and aluminum (oxide) films give good support for theoretical momentum density calculations (local-density approximation). Due to low incident electron energy the data are strongly influenced by multiple scattering effects.

The scanning transmission electron microscope or STEM, has proven to be a powerful instrument, which can combine many analytical techniques. Coincidences between x rays and energy-loss events were established in a STEM by Kruit, Shuman, and Somlyo[10] and showed the possibility of background reduction in the x-ray spectrum and the energy-loss spectrum. Unfortunately an energy-dispersive x-ray analyzer detector collects x-rays from only a limited solid angle. Together with the fact that such a detector is relatively slow, this kept them from using high count rates and therefore led to poor statistics.

Also in a STEM, Voreades[11] collected secondary electrons in coincidence with energy-loss events, but energy selection of the secondary electrons was not possible. Wittry[12] suggested to perform such energy analysis and detect specific Auger electrons in coincidence with primary electrons that have lost just enough energy to create the required inner shell hole. Compared with normal Auger spectroscopy, the coincidence detection will yield only slightly fewer counts in the Auger feature, since all emission processes of Auger electrons must be preceded by such energy losses. The background under such an Auger feature is expected to be much more reduced, since it is normally composed of tails of other Auger transitions and the secondary electron contribution from higher-energy losses, which are not selected. An equally interesting application is the idea of reducing the high background in EELS spectra in a similar way. From an increased signal to background ratio an improvement in detection limits might be expected, provided that the spectra are still statistically useful; c.f. Cazaux.[13]

In high spatial resolution STEM instruments, the magnetic field required for the fine focusing of the electron probe limited the possibility of extracting secondary electrons from the specimen and performing energy analysis on them. High collection efficiency for secondary electrons becomes possible at high spatial resolution with the introduction of the magnetic parallelizer objective lens; see, e.g., Kruit and Venables.[14] A deflector is required for separating the secondary electrons from the primary beam. The secondary electrons can then be led to an external energy analyzer.

For statistically interesting coincidence results high collection efficiency in both detectors is required. At high primary beam energies the scattering involved in the energy-loss process is confined to small scattering angles. In combination with the large range of angular demagnifications available in the STEM (necessary to ensure good matching with the analyzer), this implies that for EELS in STEM high collection efficiency is possible.

The availability of energy selection for the secondary electrons opens up many interesting possibilities for coincidence techniques. The simplest possibility discussed here, employs coincidences between energy selected secondary electrons and EELS events. Such a coincidence technique yields surface sensitive EELS information, since secondary electrons have only a very short mean free path (on the order of a few nanometers). This implies the requirement of UHV conditions, something we do not have (yet). The technique can be useful for studying the (valence) band structure. Furthermore it is of interest to determine the origin of secondary electrons.

The fact that very-high-resolution scanning images have been obtained using secondary electrons,[15] seems to contradict the delocalization that can be expected for the excitation of low energy (large wavelength) secondary electrons.[15–17] One might circumvent the problem of delocalization by observing secondary electrons only if they are accompanied by primary electrons that have lost a certain minimum amount of energy or have scattered more than a minimum scattering angle. More knowledge on secondary-electron-production mechanisms could help in explaining the observed results. A mere comparison of secondary electron information with other modes of operation of the STEM as Liu and Cowley[16] suggested, will prove useful but only in an indirect way. Experiments, which show what energy losses are responsible for the production of secondary electrons of certain energy, are expected to tell us more about the creation mechanisms. Voreades[11] collected secondary electrons in coincidence with energy-loss events, but due to the lack of energy selection for the secondary electrons he was unable to tell what production mechanisms take place. From measurements on carbon films of different thicknesses he concludes that secondary electrons are predominantly produced as a result of energy losses of about 20 eV. To decide if this happens as a result of volume plasmon decay (Gornyi[18]) or as a result of interband transitions (Willis, Fitton, and Painter[19]), he implicitly suggests the use of energy selection on the secondary electrons. Gornyi and Makarova[20] interpreted his data in terms of the decay of volume and surface plasmons, resulting in secondary-electron emission. Surface-plasmon decay dominated for thin samples, whereas volume-plasmon decay dominated for thicker samples.

This article reports on experimental coincidences between energy-selected secondary electrons and energy-selected energy-loss events. The data presented here are considered to be preliminary results of our research toward new instrumentation for high-resolution surface analysis. They have been obtained with a (S)TEM, which is equipped with a secondary-electron analyzer, an EELS detector, and some additional coincidence electronics. This instrument has been used as an electron optical test bench for a new (scanning) Auger microscope and works at an operating pressure of 10^{-4} Pa. In this vacuum any specimen is contaminated almost immediately with carbon. A thin amorphous carbon film is chosen as specimen. This way we minimize elemental changes, but we cannot avoid structural changes. One should be aware of the limitations this imposes on some of the data.

II. EXPERIMENTAL SETUP

The experiments described here have been performed on a modified Philips EM 400, which has been described

before.[14,21] Figure 1 shows the microscope in which the magnetic objective lens is equipped with a parallelizer coil, designed to produce a gradually decreasing field. This field focuses the primary (80-keV) electrons on the specimen, which is located in the high-field region. The secondary electrons, which can be emitted with large angles with the optical axis, are forced to move to the low-field region. In the low field they move much more parallel to the optical axis, and they are guided through a magnetic aperture that ends the field. The principle of the magnetic parallelizer is discussed in detail by Kruit[22] and Bleeker and Kruit.[23] After the magnetic aperture the electrons enter a 90° electrostatic deflector, with a 20-mm central radius. This deflector is placed in an extension between condenser and objective lens and has a hole in the outer sphere for the primary electrons to pass through. Electrostatic lenses guide the secondary electrons to a 180° concentric hemispherical analyzer, which has a central radius of 140 mm.

To ensure good parallelization the objective lens and parallelization coil current are set to their computed values. The specimen, which is mounted on an insulated holder, is adjusted in height to ensure focusing on the TEM screen. Fine focusing is still done with the objective lens current. The condenser lenses are used to focus a spot on the sample. The spot size on the specimen is only of the order of 1 μm, due to a nonoptimized condenser system and objective lens.

Scanning in energy for the secondary-electron analysis is performed by raising the intermediate lenses, the 90° deflector, and the 180° analyzer all with the same potential. This also means that the primary electrons are accelerated or decelerated while they pass the 90° deflector. The actual deflection they experience will therefore change with the selected secondary-electron energy. Feedback of the energy scan to the condenser deflectors minimizes this effect.

In a coincidence system, secondary-electron analysis must be performed with preservation of the timing information. Especially slow secondary electrons, which leave the sample under different angles, can experience different flight times toward the detector. To minimize this effect the sample is negatively biased (−18 V). Before the end of the parallelizer the electrons are accelerated (or decelerated) to the central potential of the 90° deflector. The pass energy for this deflector is set to 350 eV. The electrostatic lens is adjusted to get as many electrons through the entrance slit of the 180° analyzer as possible. Just before the analyzer they are slowed down to the pass energy of 100 eV.

Figure 2 shows an example of a secondary-electron spectrum of a thin carbon foil. This spectrum is obtained with the analyzer slits almost closed, so that the energy resolution is well below the intrinsic width of the secondary-electron distribution. In Fig. 3 a larger range secondary-electron spectrum is shown at a resolution of ≈ 5 eV. Due to the large dynamic range that must be covered, the vertical scale is logarithmic. At about 260 eV the carbon KVV Auger feature can be distinguished.

EELS is performed in a low camera length diffraction mode or EELS image coupling mode, which enables large scattering angles to be accepted. The GATAN 607 serial EELS system is adjusted in the usual way for a given energy resolution. Since relatively long collection times

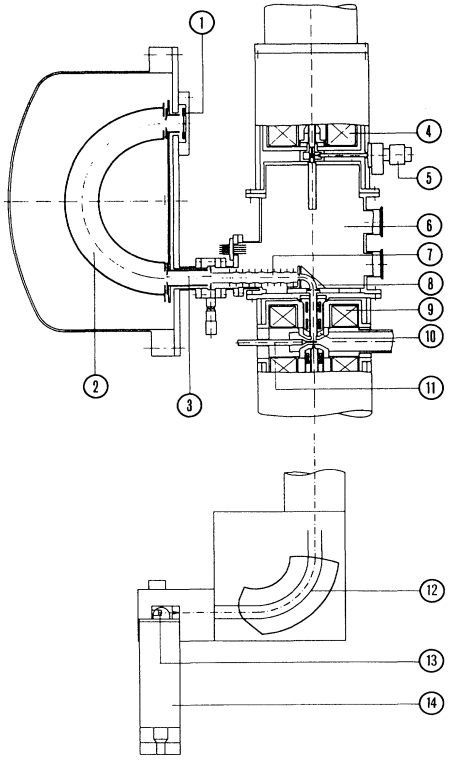

FIG. 1. Microscope column used for coincidence measurements. (1) Micro-channel-plate detector, (2) 180° analyzer, (3) beam defining slits, (4) second condenser lens, (5) condenser diaphragm, (6) microscope extension, (7) electrostatic lenses, (8) 90° deflector, (9) objective lens, (10) parallelizer coils, (11) specimen holder, (12) EELS spectrometer, (13) scintillator, and (14) photomultiplier.

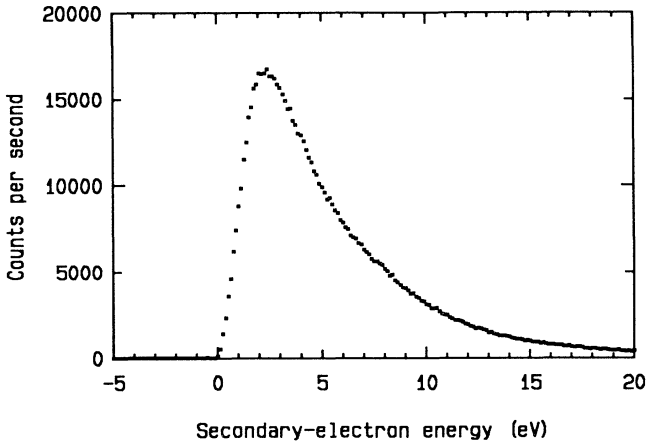

FIG. 2. Low-energy-range secondary electron spectrum from thin amorphous carbon film.

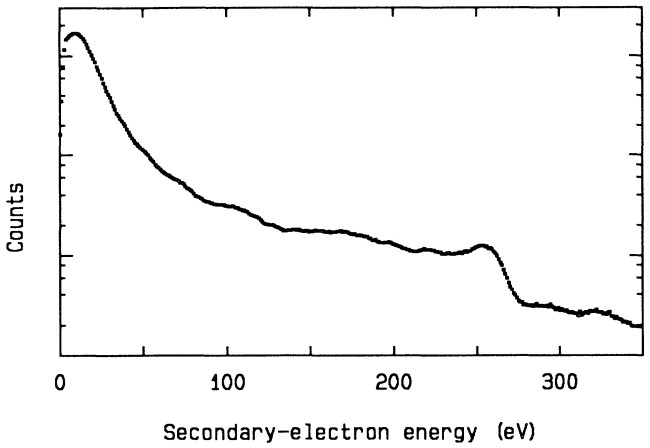

FIG. 3. Semilogarithmic plot of the secondary-electron spectrum (0–350 eV) from thin amorphous carbon film.

can be necessary in coincidence methods, drifts must be minimized. With some care drifts could be kept as low as 1 eV per 10 min.

The coincidence setup required for the described measurements is shown in Fig. 4. Of course each channel must have single-electron counting detectors. The secondary-electron analyzer is equipped with a microchannel plate detector (chevron mounted), whereas the EELS detector makes use of a plastic scintillator with photomultiplier. Electrical pulses from the anode behind the microchannel plate and from the photomultiplier of the EELS detector are led toward a time-to-amplitude converter (TAC), with a built-in single-channel analyzer (SCA). Because the anode behind the microchannel plate is at several kilovolts, an isolation transformer is used to bring the signal to ground level. A twisted pair of Teflon-coated wire-wrap wires, which have been tested to withstand voltage differences of over 5 kV, is wound several times around a ferrite coil, to give good high-frequency performance. Because of the small signal, a preamplifier is mounted almost directly behind the transformer. The signal is then led to a constant fraction discriminator, which minimizes timing inaccuracies.

The EELS photomultiplier has a built in preamplifier and constant level discriminator. In the EELS control unit a 50-Ω line driver has been added, from which the signal is sent directly to the time-to-amplitude converter. A possible improvement here would be the use of a constant fraction discriminator, instead of the constant level discriminator.

To determine if coincidences occur one first has to find out the time difference between the arrival of the electrons. For this, both detectors are set for relatively high countrates. The multichannel analyzer (MCA) accepts pulses from the TAC, which is set for a large time range, using a low primary beam current and long collecting times. The background in the spectrum represents the detection of noncoincident, unrelated electrons. A peak in the MCA spectrum represents the true coincidences. Once the peak is found, a narrow time scale such as shown in Fig. 5 can be chosen. This spectrum was obtained with narrow analyzer slits as in Fig. 2. The remaining full width at half maximum (FWHM) of 2.1 nsec, and base width of about 6 nsec, is attributed to different opening angles (leading to different flightpaths in the analyzer) and the energy range that is selected (different velocities).

To collect a coincidence spectrum the single channel analyzer (SCA) is set to accept all counts that fall in the time window, given by the base width of the true coincidence peak. The data are then collected in the multichannel scaler (MCS). Pulses output by the MCS, signifying the step to a next data channel, are used to scan

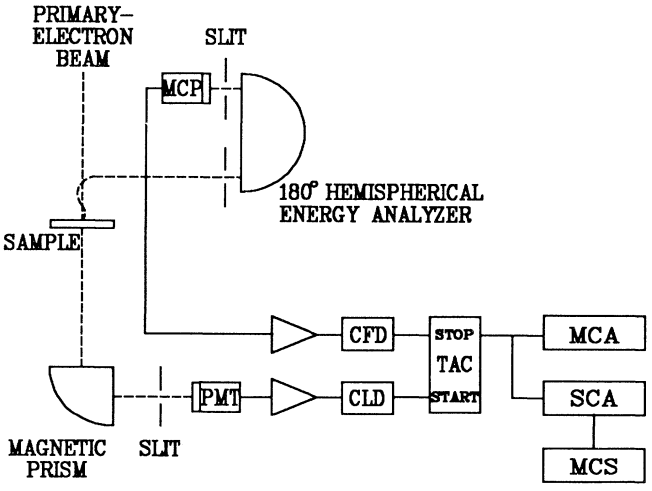

FIG. 4. Schematic coincidence set-up. MCP is the microchannel plate, PMT is the photomultiplier tube, CFD is the constant fraction discriminator, CLD is the constant level discriminator, TAC is the time-to-amplitude converter, MCA is the multichannel analyzer, SCA is the single channel analyzer, and MCS is the multichannel scaler.

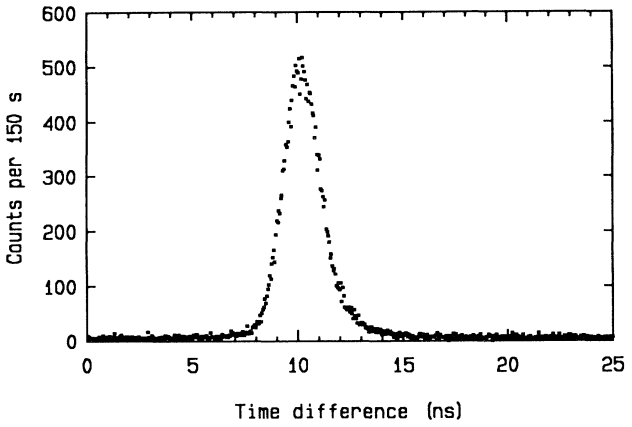

FIG. 5. MCA time difference spectrum, showing difference in arrival of secondary electrons with respect to their "creator" energy-loss electrons. Secondary electrons have an energy of 2.5 eV (this represents the maximum in Fig. 2). The energy loss selected is ≈ 16 eV.

the EELS spectrometer. A spectrum collected in this way will suffer from an energy-dependent background of false coincidences. The false coincidence count rate R_F is given by the count rate of the secondary-electron signal R_{SE} multiplied by the fraction of time that the time window is open, which is the count rate of the EELS signal R_{EELS} times the time window τ, or $R_F = R_{SE}R_{EELS}\tau$. This means that R_F has a quadratic relationship with the primary beam current I_p, whereas the true coincidence count rate R_T, just like R_{SE} and R_{EELS} behaves linearly with I_p. Together with the need for low primary beam current, it is important to keep τ as low as possible.

To determine the false coincidence background, a separate scan with different time-window setting can be made. Alternatively, this spectrum could be collected simultaneously with a differently set SCA with accompanying MCS. Since no second SCA or MCA was available, an alternate method was employed. The MCA time spectrum is recorded for a given dwell time, and the data are transferred to a microcomputer (IBM AT). In the computer a fast analysis of the time spectrum yields both true and false counts, which are both stored in memory. The scan pulses, normally output by the MCS, are now provided by the microcomputer program. They restart the process for the next energy channel. In this way the effects of primary-beam current fluctuations, or drifts of the EELS analyzer are similar for the true and false coincidence spectra.

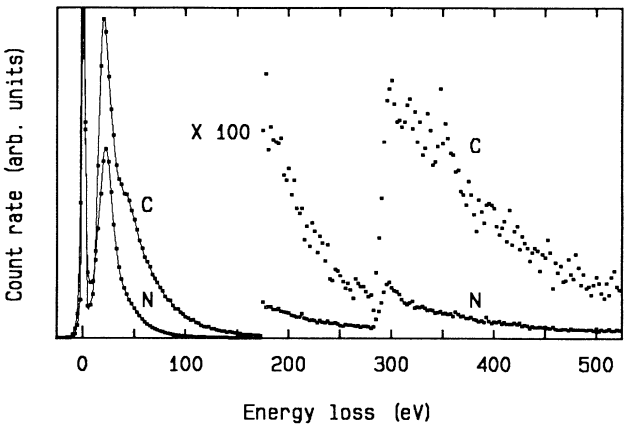

FIG. 6. Large energy range (0–500 eV) coincident (C) and normal (N) energy loss spectra. The 180° analyzer is set for the maximum of the secondary-electron distribution. The normal EELS spectrum is shown on a 200 times reduced countrate scale. Vertical full scale represents 10 000 counts per second. At 175 eV a gain change is introduced to show both the low and high range of the spectra. For both spectra the gain change is 100×.

III. RESULTS AND DISCUSSION

With the secondary-electron analyzer set to accept all secondary electrons with energy below 5 eV and the energy resolution of the EELS detector approximately set for 5 eV, a coincidence EELS spectrum is recorded. This spectrum, collected during 20 sweeps with a dwell time of 0.1 sec per channel, is shown in Fig. 6. Here no false coincidence background has been subtracted. Also shown is a normal EELS spectrum collected during two sweeps with equal dwell time. We observe some interesting differences. Just above the (false) zero loss peak the coincidence spectrum exhibits a sharper rising edge. The largest countrates occur for energy losses around 25 eV, the plasmon energy for carbon. Toward the K edge of carbon the countrate gradually decreases. However, the slope in both spectra differs considerably. The carbon K edge in the coincidence spectrum, admitting that it is more noisy, has a slightly better jump ratio, although in some measurements (not shown here) the opposite effect occurred. After the edge the coincidence spectrum does not drop as quickly as the normal spectrum. Some of the differences might be attributed to the relatively long exposure rates, which can cause beam-induced contamination. To minimize this effect, different specimen positions were selected in between the sweeps that composed the coincidence spectrum. The uniformness of the film has been checked qualitatively.

To estimate the thickness t of the film, the regular EELS data can be used. Normally[24] one would compute t from $t = -\ln(I_{zl}/I_{tot})\lambda$, where I_{zl} is the zero loss intensity, I_{tot} the total intensity, and λ the mean free path of the primary electrons for all possible energy losses. Since the height of the zero loss peak might be severely underestimated due to dead-time effects in the pulse counting process, we chose not to use this method. Instead the data have been fitted to a model function. The model is based on the jellium model for plasmon excitation, given by Egerton,[24] Eq. (3.43):

$$I_1(E) \propto \frac{E_p^2 E \Delta E_p}{(E^2 - E_p^2)^2 + (E\Delta E_p)^2} . \quad (1)$$

Fitting the EELS spectrum by means of a Levenberg-Marquardt[25] method yields the plasmon energy E_p (24.1 eV) and the FWHM of the plasmon distribution ΔE_p (18.3 eV).

From the found distribution a double-scattering distribution is computed by means of (self-) convolution and the fitting procedure is repeated, but now with double scattering included. This iterative process yields the intensity of single-(J_1) and double-(J_2) scattering distribution, from which the thickness can be estimated by $t = J_2/(2J_1)\lambda$; c.f., Egerton,[24] Eq. (4.1). For the spectrum of Fig. 6 this yields $t = 0.25\lambda$.

The mean free path λ is a mean free path for scattering events that are actually recorded, and therefore λ depends on the effective collection angle. In this experiment there is no objective aperture that limits the collection angle. We expect to collect about 10 mrad. For energy losses up to 50 eV (Egerton,[24] Fig. 3.15) we find $\lambda \approx 70$ nm, which gives $t \approx 18$ nm.

A different presentation of the data of Fig. 6 is given in Fig. 7. Here the ratio of the coincidence and normal EELS spectrum is shown, which gives a measure for the number of secondary electrons that are produced and de-

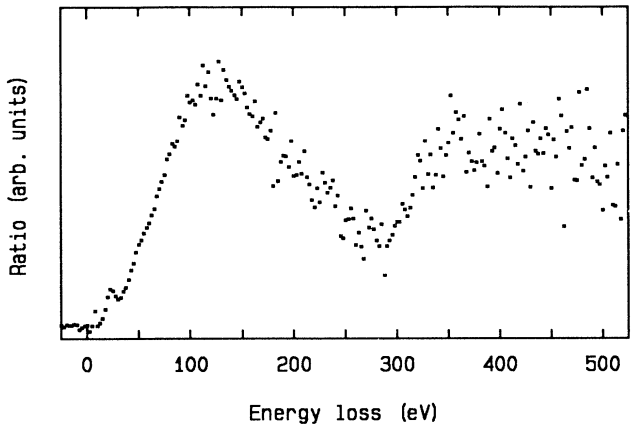

FIG. 7. Ratio of the two spectra in Fig. 6 showing the probability of low-energy secondary-electron production for a given energy-loss event. The 180° analyzer is set for the maximum of the secondary electron distribution. Vertical full scale represents a ratio of 6.25%.

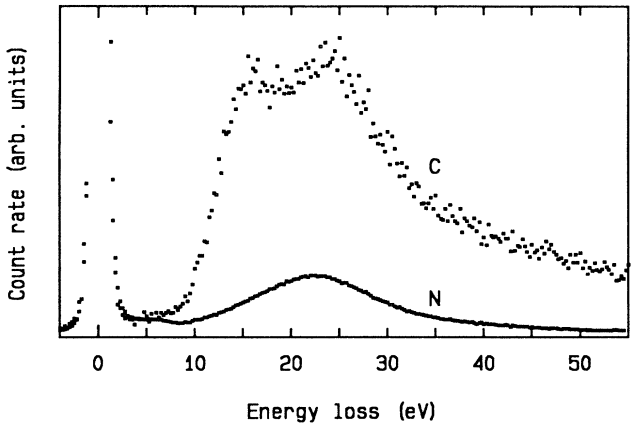

FIG. 8. Low-energy range coincident and normal energy-loss spectrum. The coincidence spectrum (C) represents energy-loss events coincident with the detection of secondary electrons of the maximum of the secondary-electron distribution. The normal energy-loss spectrum (N) is shown on the scale of the false coincidences as they appear in the coincidence spectrum.

tected per detected energy-loss event. The overall trend, from $\approx$ 25 eV up to $\approx$ 125 eV and also directly following the carbon K edge, is a linear increase in the probability of secondary-electron production, with energy loss. This trend is plausible, since with higher-energy losses more energy is available for the creation of slow secondary electrons, which agrees with the cascade description.[26] The exact processes that occur in the specimen will determine in what way and to what extent this energy is really available for secondary-electron production and emission. Emission of these secondary electrons depends on the depth in the film where the scattering takes place, the scattering directions and the mean free paths of possibly involved intermediate products. The drop in the ratio spectrum at $\approx$ 125 eV may be a thickness-dependent effect. Maybe on average the faster secondary electrons, which are directly knocked out of their atomic orbits, travel more forward (away from the top surface). This way they reach deeper before they can start a cascade that yields a slow secondary electron. The fact that different positions for the maximum in the ratio spectrum were found (not shown here) suggests the need for further studies.

In relation to the delocalization problems in scanning electron microscopy, the coincident energy-loss spectrum can be an interesting result. The different contributions to the secondary-electron detector signal can be related to the original energy-loss processes of which the degree of localization is well understood. It should then be possible to find the secondary-electron delocalization profile by summing the expected delocalization profiles for given energy loss (including the cascade effect) scaled with the height of the coincidence EELS spectrum.

We will now focus our attention to the low-energy part of the spectrum. A coincidence spectrum, collected with better energy resolution for both detectors (approximately 1.5 eV) in which the 180° analyzer is set for the maximum of the secondary-electron distribution, is shown in Fig. 8. Also shown is the normal EELS spectrum. The accompanying ratio spectrum is shown in Fig. 9. These data are taken from a different part of the specimen, of which the thickness is estimated to be 0.19λ (E_p = 24.1 eV, ΔE_p = 16.7 eV). An extrapolation of the linear slope that occurs at the right of the peak crosses the horizontal axis somewhere near 5 eV. We see a clearly distinguished peak with its center position at about a 14-eV loss and a FWHM of 6 eV. Energy losses of about 14 eV can be used for the excitation of surface plasmons. A decomposition of the normal EELS spectrum into bulk and surface plasmons by means of a Kramer-Kronig analysis (the program KKS, described by Egerton[24]), yields a surface-plasmon distribution with closely matching characteristics. It is unclear if all energy

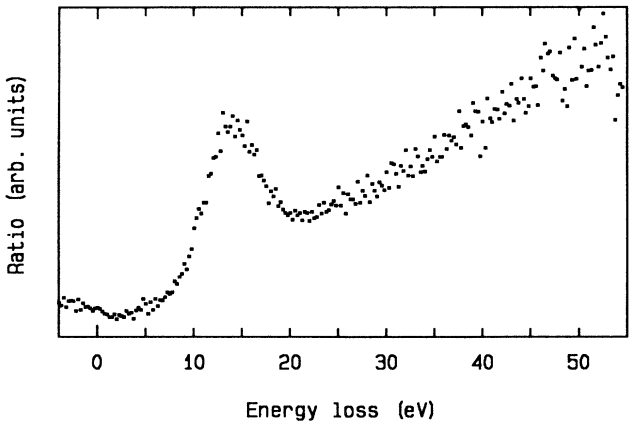

FIG. 9. Low-energy range ratio spectrum showing the prominent peak in the surface plasmon region and the general trend of a higher probability of low-energy secondary electron production for higher-energy-loss events.

of the surface plasmon must be converted to a single secondary electron (and accompanying hole), but if surface plasmons decay toward secondary electrons, roughly half of these can escape without scattering; the other half moves away to the bulk. With respect to other processes, which are not related to the surface, this gives an enhanced probability to create detectable secondary electrons.

A measure for the spatial extension of the surface plasmon[27] is the $1/e$ value of the field amplitude, which is reached at a certain depth. This depth is of the order of a few nanometers but depends strongly on the relative permittivity at the surface and the energy of the plasmon. Within such a range from the surface, the surface plasmons probably dominate over the bulk plasmons. Escaping without scattering is only possible from within the escape depth. For the selected secondary electrons, Seah and Dench[28] give a value for the mean free path of about 3 nm. Bulk plasmons are therefore unlikely to generate unscattered secondary electrons. The fact that in the ratio spectrum no trace of enhanced secondary-electron production appears at energy losses normally attributed to bulk plasmons suggests that in their decay bulk plasmons behave exactly like those electrons that are directly hit by a primary electron and then start a cascade process.

To study how the kinetic energy of the secondary electrons influences the energy-loss coincidence spectrum, a series of measurements has been done with different settings of the 180° analyzer. In Fig. 10, 15 energy-loss coincidence spectra are shown, each collected during ten sweeps with 0.1-sec dwell time per channel. Secondary-electron energy was manually set, with $\approx$ 1-eV steps, ranging from 1 to 15 eV. The original data were taken over a 128-eV range with 0.5-eV steps. Above 40-eV we observe no interesting features. False coincidence counts have been subtracted offline. The original EELS data recorded with these spectra gave the specimen thickness $t = 0.1\lambda$, the plasmon energy $E_p = 24.9$ eV and the FWHM of the plasmon peak $\Delta E_p = 19.2$ eV.

To analyze the data and to guide the eye along the spectra, fitting functions have been added. What we see in the spectra is a superposition of two features. One is a smooth peak, approximately 5 eV wide at half maximum, which seems to walk toward higher energy loss with higher kinetic energy of the secondary electron. This feature has been fitted by a Gaussian function. We observe that for the top ten spectra this peak shifts (on average) 1 eV toward higher energy loss with the 1-eV kinetic energy step of the selected secondary electrons. This suggests the interpretation of this feature as one that represents the emission of secondary electrons with equal binding energy, approximately 11 eV below vacuum level. In this way the feature is interpreted as a (virtual) photoelectron peak. Figure 11 shows the positions of the found peaks together with a line that represents a binding energy of 11 eV.

Noticeable is the slight deviation of the peak position from this linear relationship at lower kinetic energies. In fact the peak seems to stay at about 14-eV energy loss, which could indicate that the peak results from plasmon decay. The Gaussian peak then represents surface plasmons decaying into electron-hole pairs at low kinetic energies and photo electrons at higher energies. For some of the lower spectra the single-electron excitation seems

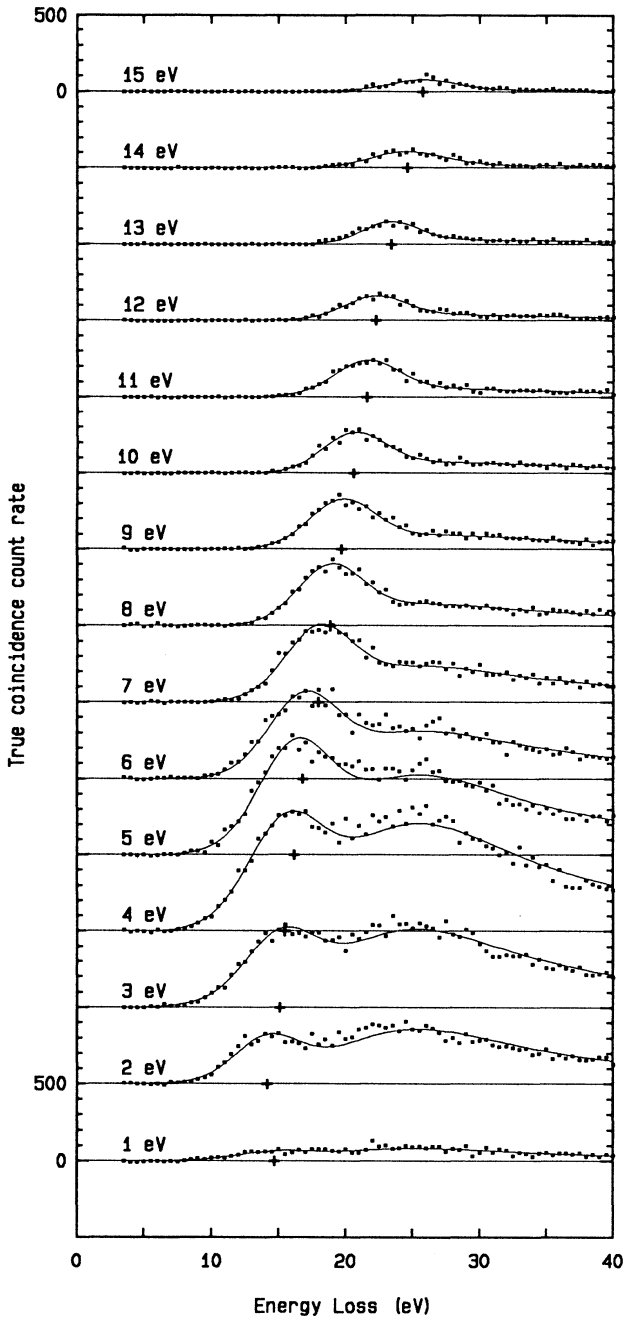

FIG. 10. Energy-loss coincidence spectra (shown as dots) for 15 consecutive values of the secondary-electron energy. Spectra have been vertically displaced over an equivalent of 500 counts. False coincidence counts have been subtracted. Secondary-electron energy was manually set, with $\approx$ 1-eV steps. Fitted functions according to the model described in the text are drawn as solid curves. The position of the Gaussian peak of this fitting model is indicated on the baseline of each spectrum (+).

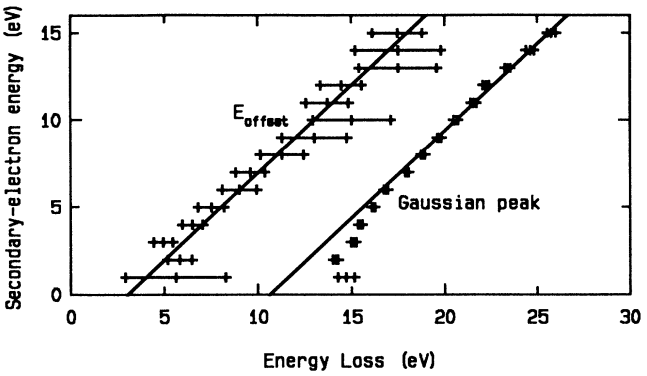

FIG. 11. Positions of the energy offset E_{offset} and Gaussian peak in the two-dimensional coincidence spectrum, as found by the fitting procedure. Error bars indicate the 95% probability interval around the computed value. Drawn lines are for $\Delta E - E_{\text{SE}} = 3$ and 10.6 eV, respectively.

enhanced by a surface plasmon excitation and the subsequent decay process.

The other feature in the spectra of Fig. 10 is a much wider nondescript bump. We know from Fig. 9 that in this region the ratio spectrum rises linear with the energy loss scale. The second feature has therefore been fitted to a multiplication of the plasmon-loss function of Eq. (1) with a factor $(E - E_{\text{offset}})$, where E_{offset} gives the minimum energy required for secondary-electron production. Below E_{offset} this function is zero. In the fitting procedure followed for Fig. 10 five parameters were free: the heights of the two features, the width and position of the Gaussian peak, and E_{offset}. Values found for E_{offset} are also indicated in Fig. 11.

Since the data are collected in a counting process, they are regarded as being Poisson distributed. The noise level on each datapoint is given by the square root of the number of counts. This forces the Levenberg-Marquardt method to "overestimate" the necessity of a good fit in regions with low count rates (and thus low absolute errors). Therefore, for some spectra the fit does not seem optimum. Some different schemes of free parameters in the fitting model can give better looking fits but make the interpretation of such a fit less clear. At least the general trend that (disregarding the lower few spectra) the positions of the Gaussian peaks form a straight line is never missing. Small deviations of the actual peak position from this line (less than ± 0.5 eV) are attributable to the manual setting of the analyzer energy and noise on the data. The deviations of the energy offset from a straight line are less than ± 1.5 eV.

Practical use of this and other coincidence techniques in the STEM still awaits high spatial resolution[29] and the clean specimen environment of a UHV microscope, which now nears completion.[30] With clean suitably chosen specimens, other coincidence techniques are at hand. High-resolution near-dipole $(e, 2e)$ spectroscopy[31] and background reduction in Auger or energy-loss spectroscopy are just a few examples.

ACKNOWLEDGMENTS

This work was part of a research program of the Foundation for Fundamental Research on Matter (FOM) and financially supported by the Netherlands Technology Foundation (STW), under Contract No. DTN 44-0745.

[1] M. J. van der Wiel and C. E. Brion, J. Electron Spectrosc. Relat. Phenom. **1**, 439 (1972/73).
[2] J. D. Jackson, *Classical Electrodynamics* (Wiley, New York, 1962), p. 719.
[3] L. Ungier and T. D. Thomas, J. Chem. Phys. **82**, 3146 (1985).
[4] I. E. McCarthy and E. Weigold, Rep. Prog. Phys. **51**, 299 (1988).
[5] H. W. Haak, G. A. Sawatzky, L. Ungier, J. K. Gimzewski, and T. D. Thomas, Rev. Sci. Instrum. **55**, 696 (1984).
[6] A. L. Ritter, J. R. Dennison, and R. Jones, Phys. Rev. Lett. **53**, 2054 (1984).
[7] Chao Gao, A. L. Ritter, J. R. Dennison, and N. A. W. Holzwarth, Phys. Rev. B **37**, 3914 (1988).
[8] P. Hayes, M. A. Bennett, J. Flexmann, and J. F. Williams, Phys. Rev. B **38**, 13 371 (1988).
[9] P. Hayes, J. F. Williams, and J. Flexmann, Phys. Rev. B **43**, 1928 (1991).
[10] P. Kruit, H. Shuman, and A. P. Somlyo, Ultramicrosc. **13**, 205 (1984).
[11] D. Voreades, Surf. Sci. **60**, 325 (1976).
[12] D. B. Wittry, Ultramicrosc. **1**, 297 (1976).
[13] J. Cazaux, Surf. Sci. **140**, 85 (1984).
[14] P. Kruit and J. A. Venables, Ultramicrosc. **25**, 183 (1988).
[15] J. Liu and J. M. Cowley, Scanning Microsc. **2**, 65 (1988).
[16] J. Liu and J. M. Cowley, Scanning Microsc. **2**, 1957 (1988).
[17] A. L. Bleloch, A. Howie, and R. H. Milne, Ultramicrosc. **31**, 99 (1989).
[18] N. B. Gornyi, Fiz. Tverd. Tela (Leningrad) **8**, 1939 (1966) [Sov. Phys. Solid State **8**, 1535 (1966)].
[19] R. F. Willis, B. Fitton, and G. S. Painter, Phys. Rev. B **9**, 1926 (1974).
[20] N. B. Gornyi and E. N. Makarova, Fiz. Tverd. Tela (Leningrad) **21**, 2187 (1979) [Sov. Phys. Solid State **21**, 1258 (1979)].
[21] P. Kruit, A. J. Bleeker, and F. J. Pijper, in *Proceedings of the European Congress on Electron Microscopy, York, 1988*, Institute of Physics Conference Series No. 93, edited by P. J. Goodhew and H. G. Dickinson (IOP, London, 1988), Vol. 1, p. 249.
[22] P. Kruit, *Magnetic Through-the-lens Detection in Electron Microscopy and Spectroscopy, Part 1*, Advances in Optical and Electron Microscopy (Academic, London, 1991), Vol. 12, p. 93.
[23] A. J. Bleeker and P. Kruit, Nucl. Instrum. Methods A **298**, 269 (1990).
[24] R. F. Egerton, *Electron Energy-Loss Spectroscopy in the Electron Microscope* (Plenum, New York, 1986).
[25] W. H. Press, B. P. Flannery, S. A. Teukolsky, and W. T. Vetterling, *Numerical Recipes: The Art of Scientific Computing* (Cambridge University Press, Cambridge, England, 1986).

[26] P. A. Wolff, Phys. Rev. **95**, 56 (1954).
[27] H. Raether, *Surface Plasmons on Smooth and Rough Surfaces and on Gratings*, Springer Tracts in Modern Physics, Vol. 111 (Springer-Verlag, Berlin, 1988).
[28] M. P. Seah and W. A. Dench, Surf. Interface Anal. **1**, 2 (1979).
[29] A. J. Bleeker and P. Kruit, Rev. Sci. Instrum. **62**, 350 (1991).
[30] A. J. Bleeker. Ph.D. thesis, Delft University of Technology, 1991.
[31] F. J. Pijper, A. J. Bleeker, R. J. Endert, and P. Kruit, Scanning Microsc. **3**, 65 (1989).